Advanced Fiber Materials (2023) 5:514–526
https://doi.org/10.1007/s42765-022-00246-4

RESEARCH ARTICLE

Boost Up the Mechanical and Electrical Property of CNT Fibers by Governing Lyotropic Liquid Crystalline Mesophases with Aramid Polymers for Robust Lightweight Wiring Applications

Ki-Hyun Ryu[1,3] · Jeong-Gil Kim[1,4] · Dongju Lee[2] · Seo Gyun Kim[2] · Bon-Cheol Ku[2] · Jun Yeon Hwang[2] · Kwang-Un Jeong[3] · Nam Dong Kim[1] · Dae-Yoon Kim[1]

Received: 16 August 2022 / Accepted: 29 November 2022 / Published online: 13 December 2022

Abstract

Monofilament type of polyaromatic amide (PA) and carbon nanotube (CNT) composite fibers is presented. A concept of a lyotropic liquid crystal (LLC) constructed via a spontaneous self-assembly is introduced to mitigate the extremely low compatibility between PA and CNT. These approaches provide an effective co-processing route of PA and CNT simultaneously to fabricate the uniform, continuous, and reliable composite fibers through a wet-spinning. Interestingly, the addition of a small amount PA into the dope solution of CNT governs the LLC mesophase not only in a spinneret stage but also in a coagulant region. Thus, the developed PA/CNT composite fibers have the high uniaxial orientational order and the close interfacial packing compared to the pure CNT fibers. The PA/CNT composite fibers achieve the outstanding tensile strength, electrical conductivity, and electrochemical response, while maintaining a lightweight. They also exhibit the chemical, mechanical, and thermal robustness. All of these advantages can make flexible, sewable, and washable PA/CNT composite fibers ideal nanocomposite materials for use in next-generation information and energy transporting system by replacing conventional metal electrical conductors.

Keywords Carbon nanotube · Aramid polymer · Liquid crystal · Composite fiber · Electrical wire

Introduction

Flexible, textile, and wearable electronics have received considerable attention due to their ubiquitous nature in everyday life and are used in mobile communication, innovation in education, healthcare monitoring, public security, and military defense [1]. The portable devices require fibers, films, fabrics, and even foams to have optical activity, electrical conductivity, and mechanical durability, while retaining user friendly nature [2]. Humans have developed high-performance fibers with novel architectures by mimicking the unique functionalities found in nature, such as the strength of ivy plants, the regeneration of lizard tails, and the shape morphing of elephant trunks [3]. Since many functional fibers have been developed for information and energy transporting applications, there are several attempts to make polyaromatic amide (PA)- and carbon nanotube (CNT)-based composite fibers in recent year [4]. PA is a class of synthetic engineering materials featuring collective hydrogen bonding and π-stacking between the molecular building blocks [5]. CNT is one of the most widely used carbonaceous

✉ Kwang-Un Jeong
kujeong@jbnu.ac.kr

✉ Nam Dong Kim
ndkim@kist.re.kr

✉ Dae-Yoon Kim
kdaeyoon@kist.re.kr

[1] Functional Composite Materials Research Center, Korea Institute of Science and Technology, Wanju 55324, Republic of Korea

[2] Carbon Composite Materials Research Center, Korea Institute of Science and Technology, Wanju 55324, Republic of Korea

[3] Department of Polymer-Nano Science and Technology, Department of Nano Convergence Engineering, Jeonbuk National University, Jeonju 54896, Republic of Korea

[4] Department of Chemical and Biomolecular Engineering, Korea Advanced Institute of Science and Technology, Daejeon 34141, Republic of Korea

conducting materials due to a giant 1D molecular structure with a high aspect ratio [6]. In these circumstances, many scientists and engineers expect that the combination of CNT and PA can further enhance or complement their physical properties like the chemical resistance, thermal stability, mechanical strength, electrical conductivity, and electrochemical performance [7].

However, the gap between experimental results and above-mentioned expectations arises from imperfect dispersion, leading the unnecessary defect, stress concentration, and interface delamination in the nanocomposites [8]. The high cohesive energy of PA and CNT due to the strong intertube interaction and close aromatic stacking, respectively, remains a major challenge in the nano-to-macroscale coassembly [9]. Most of composite fibers made of PA and CNT have a core–shell or a sheath-core structure formed by a coaxial spinning process or a multiple physical coating [10]. Therefore, it seems to be difficult to anticipate a synergistic effect of the hybridization of PA and CNT, because of their individual and decoupled layers in the macroscopic dimension. Making continuous monofilament type of PA and CNT composite fibers is hindered by the lack of scalable assembly method. Since carbon-based electrically conducting fibers have attracted a growing interest owing to the prospect of replacing metal wires, more effort is needed to overcome the low compatibility between PA and CNT [11].

Nature is adept at using a lyotropic liquid crystal (LLC) to produce the desired physical properties of the final materials [12]. For example, spiders produce uniaxially oriented and macroscopically hardened fibers with well-defined hierarchical superstructures, as their spinning dopes of protein solutions have intrinsic fluidity and inherent ordering [13]. LLC is a thermodynamically stable solution comprised of an orientational order in 1D or 2D, with partial positional order in some cases [14]. The discovery of LLC phase behaviors promises superb new approaches to utilize not only soft materials but also hard materials for the development of multifunctional materials resulting in robust and conductive textiles useful for numerous applications [15]. Xu et al. fabricated meters of macroscopic graphene oxide fibers with LLC solutions showing simultaneous lamellar ordering and long-range helical frustrations [16]. Zhang et al. developed fiber-type supercapacitors fabricated using LLC solution of MXene flakes [17]. Thus, it is realized that LLC mesophases offer a straightforward method to construct highly ordered macrostructures of 0D, 1D, and 2D materials [18].

In this study, we demonstrate, for the first time, that homogeneous PA and CNT solutions exhibit LLC phase behaviors without any supporting surfactants, binders, or stabilizers. LLC is induced only when there is a subtle balance of specific interactions in the molecular level [19]. Thus, once formed LLC phase indicates the fluidic mixture of all PA and CNT materials in a homogeneous state with a long-range order. The continuous PA and CNT composite fibers have been produced by industrially viable wet-spinning processes. The monofilament type of PA and CNT fibers possesses good mechanical performance (5.0 GPa) and high electrical conductivity (8.9 MS m^{-1}). Furthermore, the added PA plays significant role to govern the spontaneous molecular self-assembly of CNTs even in the coagulant stage. The PA and CNT composite fibers are highly sensitive to the applied stretching force, which enables the additional orientation and automatic densification of the internal structures. Since the PA/CNT composite fibers offer outstanding thermal, chemical, mechanical, and electrical properties with electrochemical performances, they provide a novel platform to investigate lightweight conductors without metals.

Experimental Section

Materials

Multiple CNT samples of Tuball (OCSiAl, single wall = 100%), XBC2340 (CCNI, single wall/double wall/multi-wall = 12%:50%:38%), EC15P (Meijo, single wall/double wall = 87%:13%), and DX2 (Meijo, single wall/double wall = 55%:45%) were used in this study. PA (964HP, moisture regain = 7%) was purchased from DuPont. Acetone (ACE, 99.5%), chloroform ($CHCl_3$, 99.8%), chlorosulfonic acid (CSA, 99.0%), ethanol (EtOH, 99.5%), hexane (HEX, 95%), hydrochloric acid (HCl, 37.0%), potassium chloride (KCl, 99.5%), sodium hydroxide (NaOH, 97.0%), and water (H_2O, ACS reagent) were purchased from Sigma-Aldrich.

Preparations

PA was vigorously washed with acetone several times, and then dried at 60 °C for 12 h under reduced pressure. CNT was thermally treated at 400 °C for 1 h by in a furnace. The spinnable LLC solution was prepared using CSA as the true solvent in a glove box. CNT and PA were carefully added into a polytetrafluoroethylene tube filled with CSA. The mixture was magnetically stirred for 72 h at room temperature and then planetary mixed for 1 h to obtain a homogeneous state. The PA/CNT composite solution as the dope was carefully transferred to a glass syringe to avoid the formation of air bubbles, and subsequently extruded through the spinneret into a coagulation bath of acetone at the dew point of − 20 °C. The PA/CNT composite fibers were rinsed in a water bath, and the resulting monofilaments were stretched and collected during the winding process. The obtained PA/CNT composite fibers on a bobbin were dried at 80 °C for 24 h in a vacuum oven.

Characterizations

The microphotographs were observed using polarized optical microscopy (POM, Nikon E600POL). The thermal behavior was monitored using the thermogravimetric analysis (TGA, TA Q50). The chemical state was analyzed by X-ray photoelectron spectroscopy (XPS Thermo Scientific K-Alpha). Field emission scanning electron microscopy (SEM, FEI Nova NanoSEM) and 3D tomography X-ray microscopy (XRM, ZEISS Xradia 810 Ultra) were used to investigate the morphology on the nanometer and micrometer length scales. To obtain the cross-sectional and longitudinal-sectional images of the fibers, a specimen was prepared using a focused ion beam SEM (FEI Helios 650). High resolution transmission electron microscopy (TEM, FEI Titan Cubed 60–300) micrographs were recorded at 80 kV equipped with an image Cs-corrector. The orientational order of the fibers was measured by Raman spectroscopy (Renishaw inVia Reflex) equipped with a polarizing filter. The single fiber tester (Textechno FAVIMAT) was used to measure the mechanical properties of the fibers. Knot efficiency was calculated by dividing the breaking strength of knotted by that of flat fibers to further evaluate mechanical properties. A probe station with four-point probe (MS Tech MST-4000A) was employed to measure the electrical properties of the fibers. The electrochemical properties of fiber electrodes were analyzed by the electrochemical workstation (CHI 920D) in three-electrode system. The reference electrode and counter reference electrode were Ag/AgCl (saturated 3 M KCl) and a Pt mesh, respectively. A single fibrous electrode of 5.5 cm long was used as the working electrode. The electrochemical characteristics were measured using the cyclic voltammetry (CV, scan rate $50 \le v \le 10$ k mV s^{-1}), galvanostatic charge/discharge (GCD, $1 \le J \le 50$ A g^{-1}), and electrochemical impedance spectroscopy (EIS, frequency range from 0.01 to 100 kHz, amplitude of 0.01 V). The density of the fiber was obtained using a gradient density column.

Results and Discussion

CSA was selected as the most proper solvent among many others options, including nitric acid, hydrochloric acid, sulfuric acid, and phosphoric acid, because it can disperse both PA and CNT effectively [20]. The target amounts of PA and CNT were added to a glass vial and dispersed uniformly in CSA solution (Fig. 1a). A series of the PA/CNT solutions with different CNT contents (100/0, 90/10, 80/20, 70/30, 60/40, 50/50, 40/60, 30/70, 20/80, 10/90, and 0/100) were prepared with the LLC dope for used in the wet-spinning process. The vials filled with PA/CNT solution at 8 mg mL^{-1} showed clear and black coloration observed by the naked eye, which indicated that PA and CNT were well-dissolved in the CSA (Fig. S1).

The LLC phase behaviors of the PA/CNT solutions were determined by using POM. All were optically anisotropic.

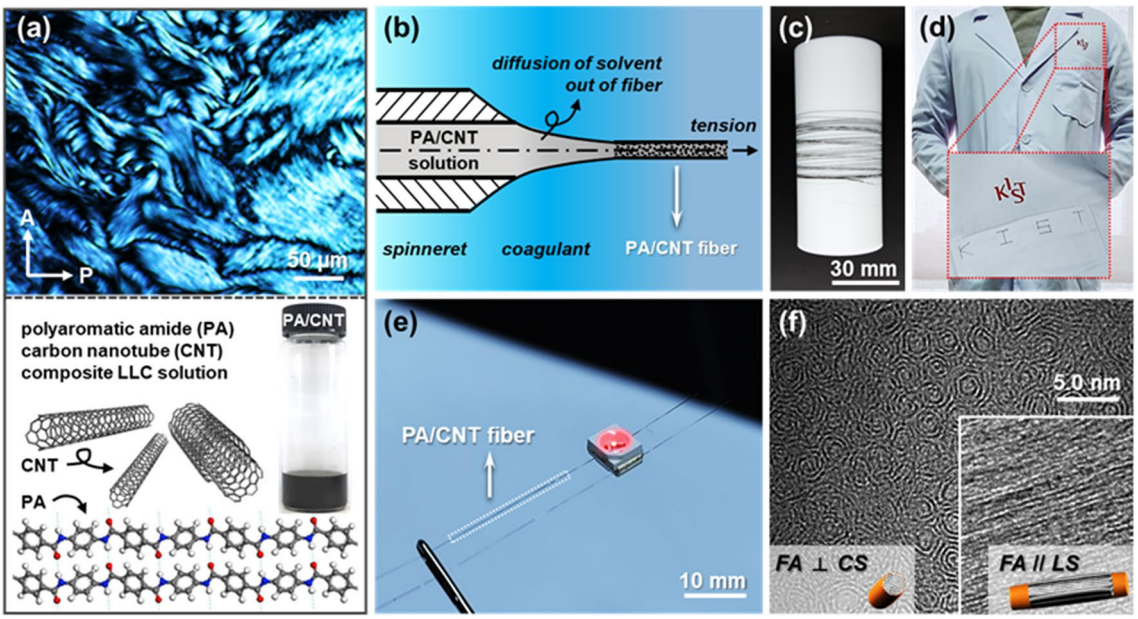

Fig. 1 Macroscopic photograph of the homogeneously mixed PA/CNT solution and its LLC phase behaviors (**a**). Schematic illustration of the construction of the uniaxially oriented composite fibers via the wet-spinning process (**b**). Continuous PA/CNT fibers wound on the bobbin (**c**). Photograph of lab coat weaved with PA/CNT fibers (**d**). Demonstration of light-on-fiber by connecting two PA/CNT fibers to a direct current (**e**). TEM images measured at viewing angles of perpendicular and parallel direction to the PA/CNT fiber long axis (**f**)

The dope depolarized plane polarized light and exhibited opalescence at room temperature due to the absence of undissolved solids (Fig. S2). Nematic phases were identified by thread-like topological defects known as Schlieren textures [21]. Observation of significant birefringence indicated that the one-pot LLC formulation method using PA and CNT had overcome the solubility and compatibility issues. Additionally, the absence of additives in the LLC solution like surfactants, binders, or stabilizers, that often act as a defect in the composite materials lowering the physical properties, should be useful to obtain the processibility for mass production [22].

The PA/CNT solutions were subjected to wet-spinning through a fine nozzle into a coagulation bath using a custom-made spinning rig (Fig. 1b). After washing and subsequent drying, the continuous monofilament type of the PA/CNT fibers were collected with a bobbin (Fig. 1c). Note that the PA/CNT (100/0) fibers had a yellowish coloration. The fibers darkened to grey and then black as their CNT content increased (Fig. S3). SEM image shows that the thickness of the PA/CNT fibers was approximately 15 μm in diameter (Fig. S4). The excellent flexibility of the PA/CNT fibers endowed them with outstanding machinability, for tasks such as weaving, sewing, and knitting (Fig. 1d). The PA/CNT fiber was easily sewed onto a lab coat using a running stitch (Fig. S5). The PA/CNT fiber was handled without breaking and withstood to the applied force of being stitched.

Since the PA/CNT fibers conducted electricity, the light-on-fiber was demonstrated (Fig. 1e). Two strained PA/CNT fibers were supported by the hole of a needle. When the LED chip was loaded onto two PA/CNT fibers, maintaining a certain distance, it revealed a red light by forming the current flow. Two monofilament of 10.0 cm PA/CNT fibers whose mass totaled 0.042 mg were able to hold the 32.4 mg weight of an LED chip, which was over 771 times the weight of the fiber. The cross section (*CS*) and longitudinal section (*LS*) of TEM image of the PA/CNT fibers indicate that LLC assists the separation of the entangled molecules, improving their dispersibility (Fig. 1f). In addition, the microstructure of the PA/CNT fibers had uniaxial orientation of the molecules along the fiber axis (*FA*).

The flexible and strong PA/CNT fiber is capable of being tied into a knot and twisted into a braid. SEM images show various morphological distortions of the PA/CNT fibers, including flat, knotted, and twisted shapes (Fig. 2a). The PA/CNT fibers had a high degree of flexibility, which enabled easy bending and a high knot efficiency of 82.67% (Fig. 2b). This high degree of flexibility is not normally seen in high-performance fibers like Nylon (polyamide fiber), Dyneema (polyethylene fiber), and T300 (carbon fiber) [23]. The 2-ply and 3-ply twisted PA/CNT fibers maintained their original flat shape without collapsing. The tensile strength of the twisted fibers was almost identical to that of the monofilament strand, because their cross-sectional area had nearly doubled and tripled, respectively (Fig. S6). However, when the PA/CNT fibers were twisted with two and three strands of monofilaments, the resulting tensile load was 1.82 and 2.78 times higher than that of the as-spun initially flat-shaped single strand fiber. This indicates that the braiding process strengthened the fiber tufts.

The flexible PA/CNT fibers can serve as a thread for sewing by following the running stitch. As shown in Fig. 2c, the PA/CNT fibers were sewed onto a conventional Kevlar mat. The optical microscopy image shows that the PA/CNT fiber was well-integrated without any cracks or deformations (inset of Fig. 2c). Interwoven networks of the PA/CNT fibers offered excellent washability. Washing is performed by a simulated washing with continuous stirring and a washing machine with standard procedure (Fig. S7). The resistance variation showed that the PA/CNT fibers maintained their electrical properties and original shapes after several washing cycles, which indicated that they can be used in flexible and wearable electronics applications. Figure 2d showed the copy-paper-based electronics with eight fibers of the PA/CNT fibers lighting up twenty-four LED chips comprising the word "KIST".

The mechanical properties of the PA/CNT fibers prepared with different PA and CNT weight ratios were evaluated using a tensile test (Fig. 2e). The actual loading force to the PA/CNT fibers is presented in Fig. S8, and the maximum tensile load gradually improved to 57.11 cN. The specific tensile strength of the PA/CNT (10/90) fibers (2.71 N tex^{-1}) was 5.5 times higher than that of the PA/CNT (90/10) fibers (0.49 N tex^{-1}), while elongation at break remained constant. The toughness of the PA/CNT fibers also improved as the CNT content increased (Fig. S9). The added CNT played a significant role in improving composite fiber strength, because of its intrinsic high molecular stiffness and rigid rod-like geometry [24]. While the hybridization of polymers with nanofillers improves their mechanical properties, such results are only achieved when CNT is homogeneously mixed with the PA matrix [25]. When the PA/CNT (10/90) fibers were spun with heterogeneous mixtures agitated for only 1 h, they exhibited lower tensile strength and elongation at break than those prepared using the LLC dope with a sufficient agitation time of 72 h (Fig. S10). Note that the solution of PA and CNT mixed for less than 1 h did not form continuous fibers during the wet-spinning process. The irregular agglomerations of CNT that resulted from the phase separation led to a loss in close interfacial interactions with PA and thereby caused defects in the internal structures (Fig. S11). The stabilization of the uniform domain in the phase structures via LLC self-assembly can thus enable the development of advanced composite fibers made of low-compatible materials.

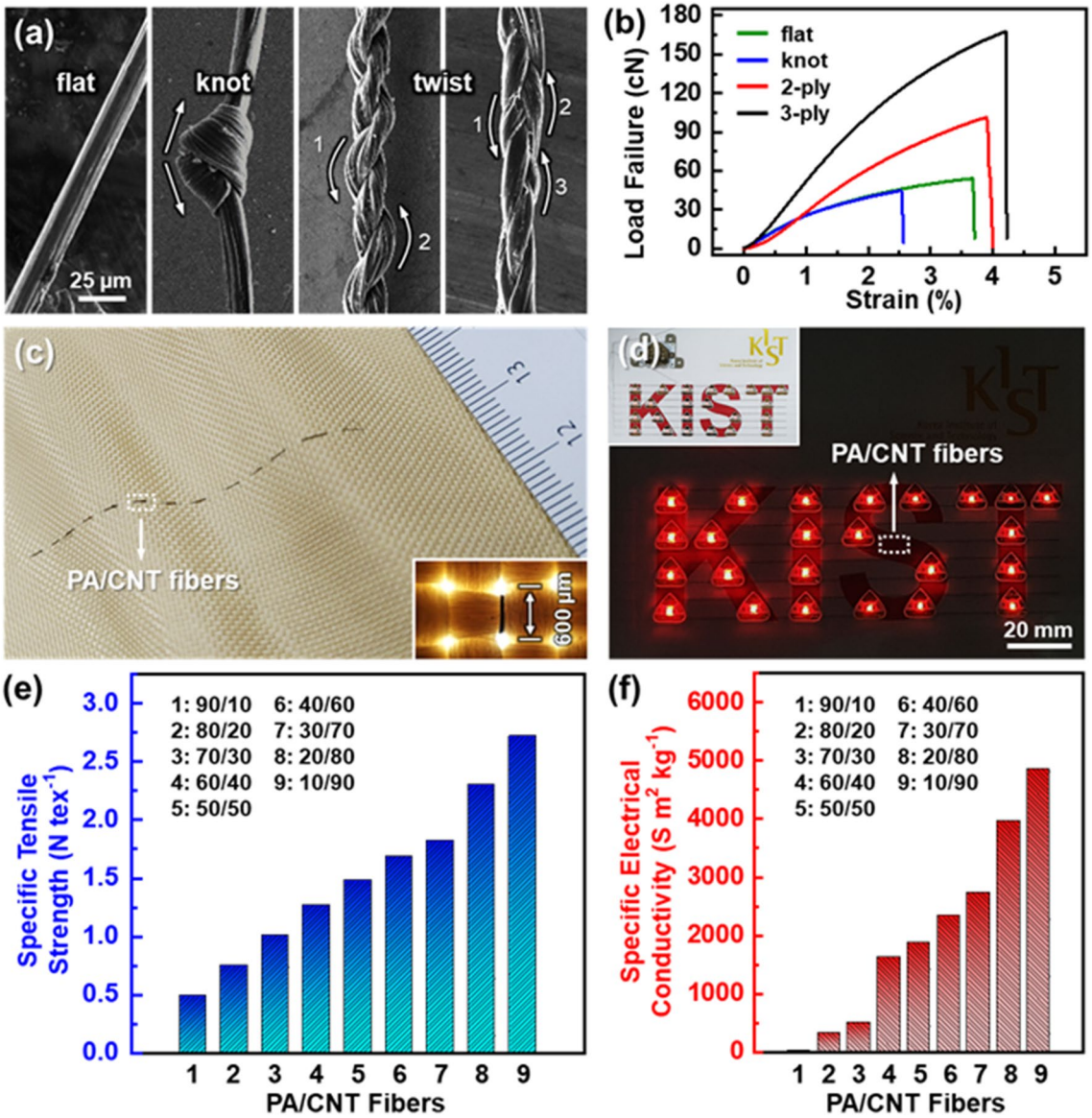

Fig. 2 SEM images of the flat, knot, and twist shape of the PA/CNT fibers (**a**) and their mechanical behaviors (**b**). Photograph and optical microscopy images of the PA/CNT fiber woven onto a conventional Kevlar mat by running stitch through the needle (**c**). LED array using the PA/CNT fiber wiring (**d**). Specific tensile strength (**e**) and specific electrical conductivity (**f**) of the PA/CNT fibers

The PA/CNT fibers contained almost exactly the target amounts of PA and CNT, as a result of the accurate dispersion by means of LLC mesophases, which facilitated the tuning of physical properties. The thermogravimetric analysis (TGA) indicated that the remained weights at 650 °C were improved from 9.43% to 86.25% of the PA/CNT fiber when the content of CNT was increased to PA (Fig. S12). After selective thermal degradation of PA, the residual weight ratio of the PA/CNT fiber was well matched to the content of CNT, which was added in the LLC spinning dope. Further analysis was performed by using the X-ray photoelectron spectroscopy (XPS), which was a sensitive and quantitative method to figure out the elemental composition. As shown in Fig. S13, O1s and N1s peak was appeared at 533.4 eV and 400.1 eV, respectively. The relative atomic content of C was increased by the addition of CNT, while the peak intensity of O and N attributed to the amide function of C=O and N–H in PA was concomitantly decreased. Note that C1s peak at 285.2 and 284.5 eV corresponded to the C–C and C=C bond of the aromatic ring. The FT-Raman spectra analyses of the PA/CNT fibers showed the combined characteristic peaks of D- and G-band from CNT and amide-I and -II function from PA (Fig. S14). The PA and CNT can be fully dissolved by, yet resist decomposition from, the true solvent of CSA,

allowing the large-scale production of the highly reliable PA/CNT composite fibers.

The addition of CNT effectively improved the electrical conductivity of the PA/CNT fibers (Fig. 2f). As the CNT content increased, the PA/CNT fibers exhibited a significant decrease in the resistance from 2.31 kΩ to 0.0098 kΩ (Fig. S15). The specific electrical conductivity of the PA/CNT fibers increased with the weight fraction of CNT. A specific electrical conductivity over 4,859 S m^2 kg^{-1} was achieved with 90% CNT content in the composite fiber. The increased electrical conductivity of the PA/CNT fibers can be attributed to the continuous electrical conducting pathway along the uniaxially oriented CNT domains in PA matrices [26]. Since the PA/CNT (10/90) fiber had the highest value of tensile strength and electrical conductivity compared to the other composite fibers that were tested, we focused on the PA/CNT (10/90) solution to determine the most effective macroscopic properties.

The PA/CNT (100/0) fibers were electrically insulating, and we thus compared the physical properties of the PA/CNT (10/90) and PA/CNT (0/100) fibers. The enhancement in physical properties we observed after adding only a small amount of PA into the CNT solution was unexpected, because unlike CNT, PA is neither a strong material in theory nor an electrical conductor in practice as against CNT [27]. Note that the PA/CNT (0/100) fibers were fabricated using the same temperature (24 °C), relative humidity (13%), concentration (8 mg mL^{-1}), coagulation (acetone bath), neutralization (water bath), and draw ratio (3.0) during the wet-spinning procedure. They exhibited an electrical conductivity of 3,537 S m^2 kg^{-1} (Fig. S16). A specifically designed experiment was conducted by POM to understand why seasoning the PA into the CNT showed more advantageous physical properties for composite fibers.

A drop of PA/CNT (10/90) and PA/CNT (0/100) solution in the LLC phase was deposited into one-hole slide glass filled with acetone. Then, an optical cell was covered by sandwiching the glass substrate with 10 μm spacers and sealing it with an epoxy resin. When the LLC solution for PA/CNT (0/100) in N phase met the acetone, large numbers of CNT precipitated to form a highly aggregated CNT island on the isotropic liquid of the solvent mixtures (Fig. 3a). The spinning dope from the PA/CNT (0/100) immediately solidified in the coagulant, and it was no longer in the LLC phase which indicated the disappearance of birefringence. However, the PA/CNT (10/90) solution still showed the strong birefringence under POM observation, before and immediately after immersion into the coagulating solvent (Fig. 3b). Several micrometer sized particles were detected, but the randomly oriented multifold LLC domains were coexistent [28].

Regarding the PA/CNT (10/90) fibers, the slow diffusion of CSA into acetone delayed the solidification of LLC domain, as the local hydrogen bonding trapped the molecules between the donor and acceptor function. The monofilament of the PA/CNT (10/90) fiber was unable to

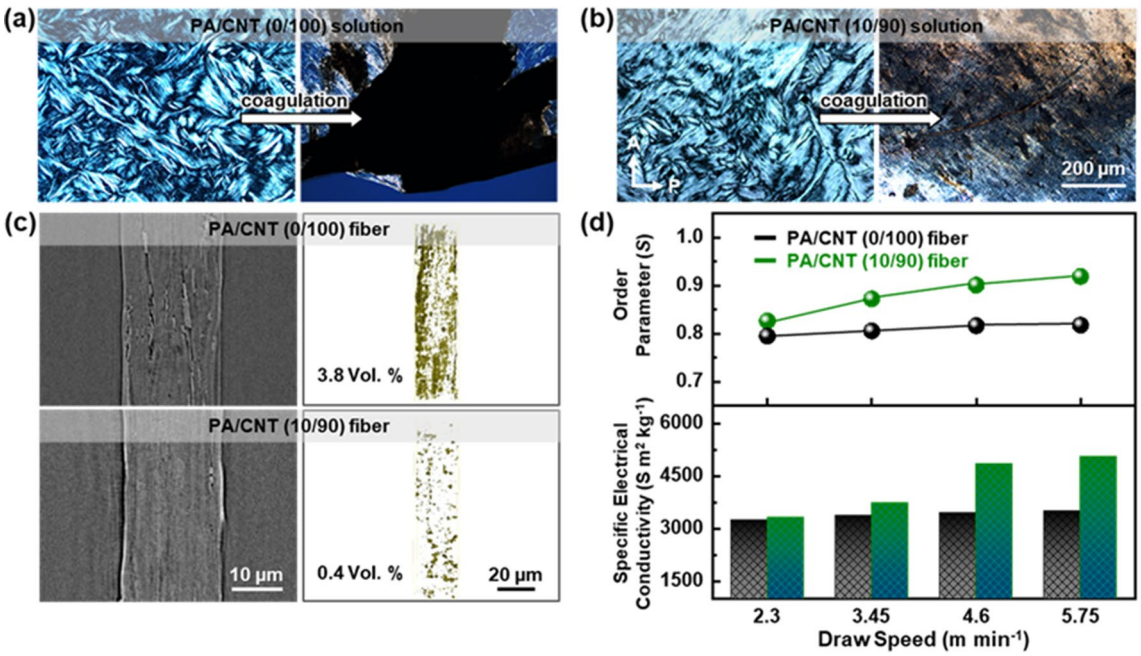

Fig. 3 POM images of the spinning dope for PA/CNT (0/100) solution (**a**) and PA/CNT (10/90) solution (**b**) before and after the coagulation process. XRM images of PA/CNT (0/100) fiber (top) and PA/CNT (10/90) fiber (bottom) and their internal structure visualization (**c**). Electrical properties and order parameter of PA/CNT (0/100) fiber and PA/CNT (10/90) fiber prepared at the different *DS* (**d**)

immediately solidify even in the spin-line. The PA/CNT (10/90) fiber maintained the motionable features for the molecules and chain segments. Therefore, the remaining LLC behaviors in the coagulant assisted the uniaxially arranged and densely packed structures when the stretching force was applied along *FA*. Thus, the order parameter (*S*) of the PA/CNT (10/90) fibers were sensitive to the draw speed (*DS*) of the winding roller (Fig. S17). The maximum *S* of the PA/CNT (10/90) fiber is determined to be 0.919. Conversely, the immediate loss of fluidity of the long-range order in 1D hampered the extra uniaxial orientation of PA/CNT (0/100) fiber during the drawing process. The fast exchange of the spinning solution into the coagulant froze the molecular mobility. Therefore, the molecular alignment only occurred in the spinneret region which resulted in the low dependence of the tensile stress on the *DS* (Fig. S18). The PA/CNT (0/100) fiber had only the tensile strength of 1.66 N tex^{-1}. In addition, the maximum *S* of PA/CNT (0/100) fiber was 0.818 which was almost similar to the lowest *DS*, even though the *DS* was 2.5 times higher than the initial take-up speed (Fig. S19).

The microstructural changes of PA/CNT (10/90) fibers and PA/CNT (0/100) fibers were visualized by XRM. Using non-destructive 3D X-ray imaging, the internal voids on the scale of hundreds of nanometers to tens of micrometers were quantified without artifacts (Fig. 3c). At the same *DS* of 5.75 m min^{-1}, a low volume percent of void (0.40 vol%) was observed along the *FA* of the PA/CNT (10/90) fibers compared to the PA/CNT (0/100) fibers (3.80 vol%). The high alignment prevented the poor interfacial contact while the low orientation rendered the molecular packing difficulties. The reduced voids with the help of enhanced *S* decreased the distance between the internal bundles that controlled the electron transport scattering site and load transfer defect density in the composite fibers (Fig. 3d) [29].

To understand the enhanced physical properties of the PA/CNT fibers, the electrocapacitive performance was also evaluated. The electrochemical response of the PA/CNT (0/100) fibers yielded a quasi-rectangular shaped cyclic voltammetry (CV) curve (Fig. S20). The undistorted triangular shaped galvanostatic charge/discharge (GCD) profile proved the highly capacitive characteristics of PA/CNT (0/100) fiber [30]. It is noteworthy that the capacitive characteristic of PA/CNT (0/100) fiber was well-maintained even up to a scan rate of 10,000 mV s^{-1}, which highlighted the good electrical conductivity itself. For PA/CNT (10/90) fibers, the shapes of the CV curves were not rectangular with potentials peaks of 0.25 V, 0.42 V, and 0.81 V (Fig. S21). However, the PA/CNT (10/90) fiber showed a much larger CV curve than the PA/CNT (0/100) fiber (Fig. 4a). These enhanced

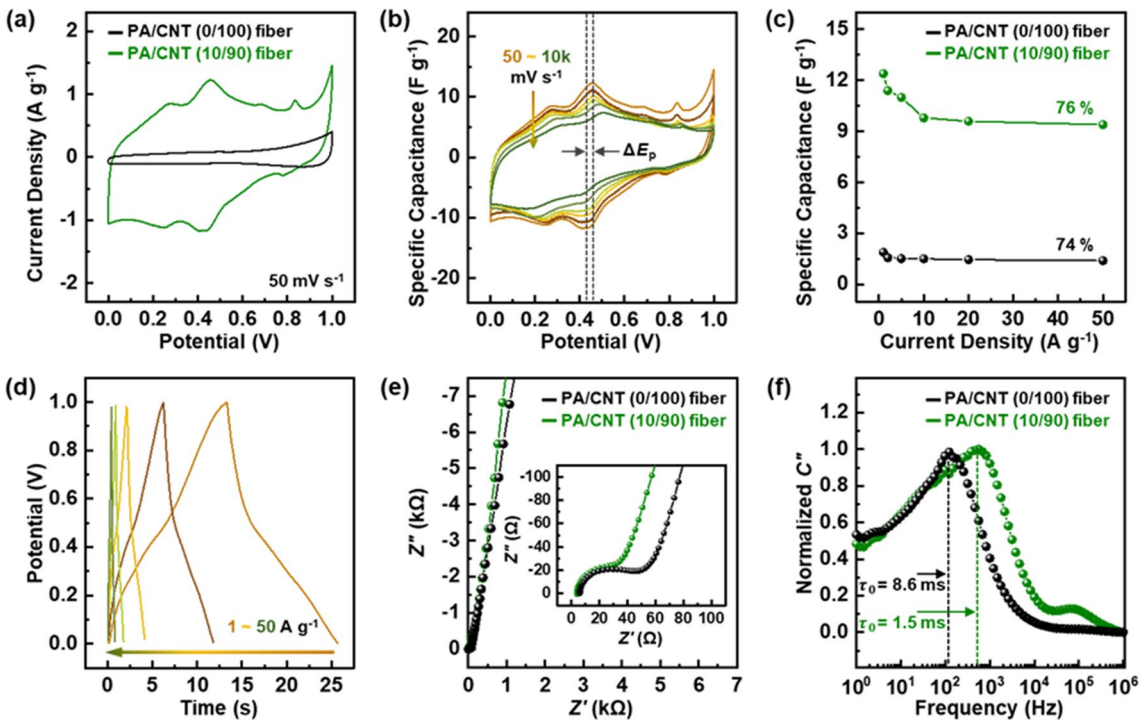

Fig. 4 CV profiles of the PA/CNT (0/100) and PA/CNT (10/90) fibers (**a**). CV curves of PA/CNT (10/90) fiber at scan rates from 50 to 10,000 mV S^{-1} (**b**). Specific capacitance of the PA/CNT (0/100) and PA/CNT (10/90) fibers at different current densities (**c**). GCD curves of the PA/CNT (10/90) fiber (**d**). Nyquist plots obtained from the EIS analysis of the PA/CNT (0/100) and PA/CNT (10/90) fibers (**e**). Normalized imaginary parts of the complex capacitances of the PA/CNT (0/100) and PA/CNT (10/90) fibers (**f**)

capacitance properties were well-maintained even at a very fast scan rate of 10,000 mV s^{-1} (Fig. 4b). The cathodic and anodic peak potential separation (ΔE_p) was an indicator of the redox kinetics of electrode materials [31]. Notably, the PA/CNT (10/90) fiber maintained very small peak potential separation even at a scan rate of 1000 mV s^{-1}, which implied a highly reversible and fast redox reaction kinetic (Fig. S22). The PA/CNT (10/90) fiber (12.4 F g^{-1} at 1.0 A g^{-1}; 9.4 F g^{-1} at 50.0 A g^{-1}; rate retention of 76%) showed much higher electrochemical performance than the PA/CNT (0/100) (1.9 F g^{-1} at 1.0 A g^{-1}; 1.4 F g^{-1} at 50.0 A g^{-1}; rate retention of 74%) as shown in Fig. 4c and d.

To analyze the superior performance of the PA/CNT (10/90) fiber, the electrochemical impedance spectroscopy (EIS) is used. Figure 4e showed a Nyquist plot in a frequency range from 100 kHz to 0.05 Hz. In the high frequency region, both samples showed similar equivalent series resistance values, but the PA/CNT (10/90) fiber exhibited a much smaller charge transfer resistance (36 Ω) than the PA/CNT (0/100) fiber (45 Ω), revealing its highly conductive properties [32]. In the low-frequency region of Warburg impedance, the PA/CNT (10/90) fiber exhibited slightly lower ion diffusion resistance than the PA/CNT (0/100) fiber, featuring facile ion diffusion characteristics. As shown in Fig. 4f, the PA/CNT (10/90) fiber shows excellent frequency response with very small relaxation time constant of 1.5 ms (τ_0 being the minimum time required to discharge all of the energy with $a > 50\%$ efficiency) resulting from the outstanding charge transfer and ion diffusion and transport kinetics. The highly enhanced electrochemical properties of composite fibers by addition of PA into CNT should be attributed to (i) the low electrical resistance as well as a high-rate performance, and (ii) the improved wettability as well as the facile redox reaction [33]. The construction of composite structure from PA and CNT was beneficial for the power and energy performance related to the electrical resistance and specific capacitance.

To further enhance the physical properties of the PA/CNT (10/90) fibers, the phase structures of the LLC dope depending on the concentration were determined (Fig. 5a). The intermolecular interaction in the molecular level influenced not only in the microscopic level but also in the macroscopic level of the PA/CNT (10/90) fibers. Under POM, the PA/CNT (10/90) solution at the room temperature showed a complete dark state indicating the isotropic (ISO) liquid state with the short-range molecular order. The isotropic cloud point (ICP) was observed as 0.14 mg mL^{-1}, which indicated the start of the self-assembled LLC domain growth. The continuous PA/CNT (10/90) fiber did not form when the concentration of solution was below the ICP. This finding showed that the close intermolecular interaction between the PA and CNT should not be sufficient to produce the composite fibers in the ISO and ICP regions.

When the concentration was increased from 0.14 mg to 6.0 mg mL^{-1}, the biphasic (BI) state was formed. The PA/CNT (10/90) solutions can be spun when the concentration reached to the BI state. However, the *S* of PA/CNT (10/90) fiber prepared in the BI state was lower than the N state because of the existence of a liquid part that affected the long-range molecular order of the LLC domain (Figs. 5b and S23). They did not bear full load, reducing the mechanical strength. In addition, the disruption of alignment can increase the junction resistance [34]. Further increasing the concentration over 6.0 mg mL^{-1}, the N domains grew and joined together to form a single phase, and showed typical Schlieren textures with the black brushes. It was only when the PA/CNT (10/90) fibers reached N, did they show stable physical properties (Fig. 5c). The tensile strength and electrical conductivity were nearly saturated at 8.0 mg mL^{-1} in the N phase.

To verify how the aspect ratio (*AR*) of CNT affects the physical properties, four different CNTs were used to fabricate the PA/CNT (10/90) fibers. The ICP of CNT in CSA was determined as the midpoint between the most concentrated solution without birefringent and the least concentrated solution with birefringent (Fig. S24). The measured ICP was inversely related to the *AR* of CNT. On the basis of Onsager scaling, the *AR* of four different CNTs were measured to be 1084, 1747, 2996, and 5817 (Fig. 5d) [35]. As shown in Fig. 5e, the specific tensile strength of PA/CNT (10/90) fiber was proportional to the *AR* of CNT. The longer *AR* of CNT can result in higher surfaces for load transfer, a lower defect density, and fewer CNT junctions per unit of fiber length [36]. Based on the established linear trend between *AR* of CNT and the physical properties, the PA/CNT (10/90) fiber fabricated from CNT with the $AR = 8000$ are expected to possess 3.65 N tex^{-1} and 6,189 S m^2 kg^{-1} by a simple extrapolation. Since the specific electrical conductivity of copper (Cu) wire is 6,500 S m^2 kg^{-1}, the current result of the PA/CNT (10/90) fiber can dedicate for development in the field of electrical conductors with no metal present [37]. From this perspective, the optimized PA/CNT (10/90) fibers accompanied with the low-cost and large-scale fabrication can be considered as a common conducting wire in the near future.

Since the physical properties of the PA/CNT (10/90) fibers are sensitive to the *DS* owing to the presence of LLC behaviors judged by the maximum *S* (0.919) and the electrical conductivity (5044 S m^2 kg^{-1}) at 5.75 m min^{-1}, applying stretching force to the PA/CNT (10/90) fibers towards the spin line direction also leads the improved mechanical properties. We observed that increasing the *DS* of the winding roller from 2.30 to 5.75 m min^{-1} enhanced the specific tensile strength of the PA/CNT (10/90) fibers from 1.49 to 2.82 N tex^{-1} (Fig. 5f). The stretching force effectively aligned the PA/CNT (10/90) fiber which resulted in a proper

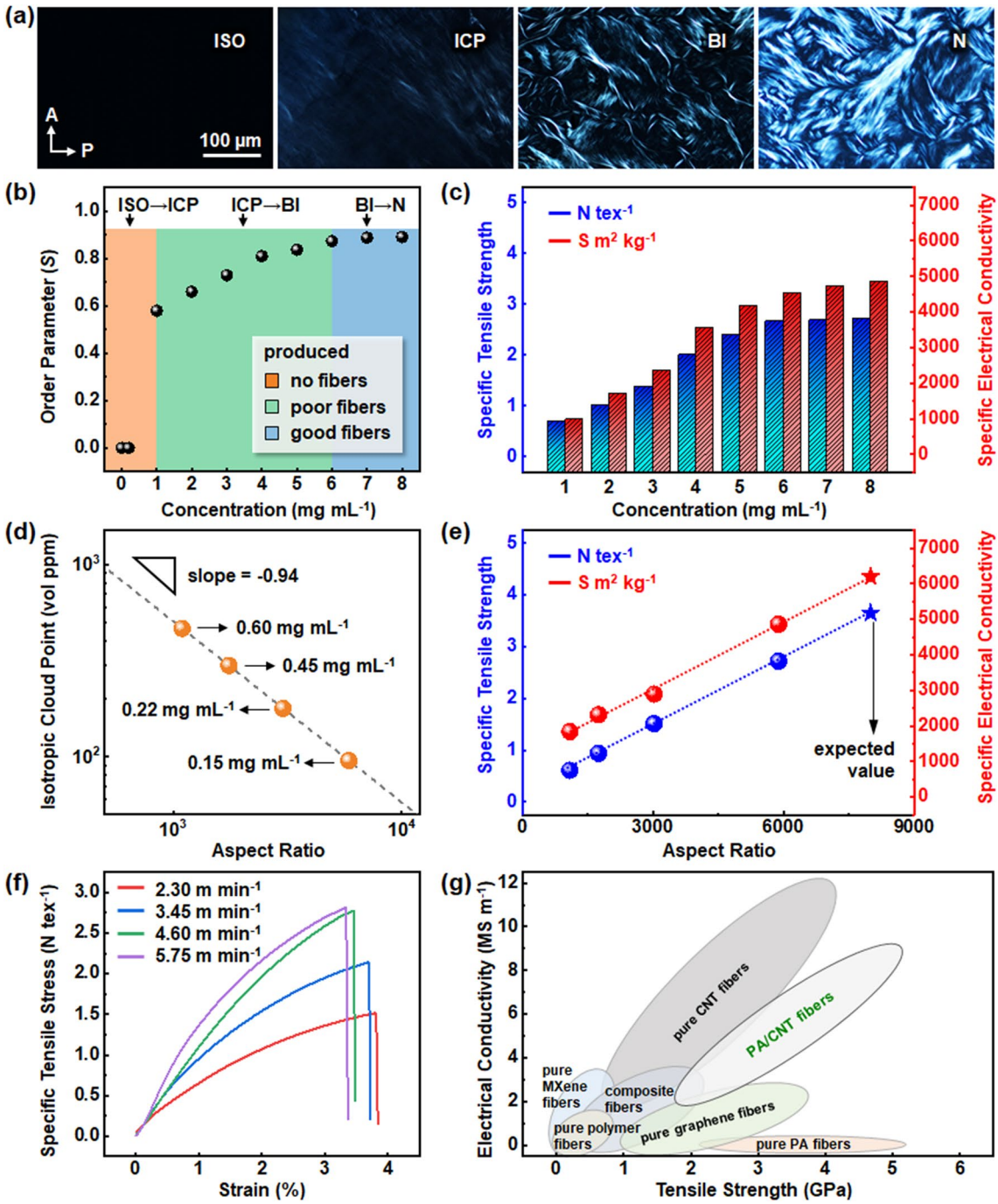

Fig. 5 Molecular self-assembly feature of the PA/CNT (10/90) solution observed by POM images (**a**). *S* changes of the PA/CNT (10/90) fibers spun at ISO, ICP, BI, and N phase regions (**b**). Mechanical and electrical properties of the PA/CNT (10/90) fibers depending on the ordered states of spinning dopes (**c**). Phase behaviors of CNT as a function of *AR* and concentration (**d**). Tensile strength and electrical conductivity of the PA/CNT (10/90) fibers fabricated with the different *AR* of CNT (**e**). Changes to the mechanical properties of the PA/CNT (10/90) fibers upon increasing the *DS* (**f**). Tensile strength of the PA/CNT fibers against electrical conductivity plotted on an Ashby plot together with other wet-spun fiber materials (**g**)

ordering and internal packing compared to fibers subjected to a lower stretching force. Therefore, it is apparent that the drawing process can be considered as a primary determinant of the physical property of the PA/CNT (10/90) fiber. In addition, the introduction of the fast *DS* contributed significantly to productivity growth. It should be noted that the PA/CNT fibers used in the present experiments were prepared manually in a laboratory. The optimizing the processing of

PA/CNT, which requires high levels of multiple coagulating, stretching, annealing, and sizing steps, will lead to dramatic improvements in physical fiber properties.

The tensile strength of commercially available pure PA fibers such as Kevlar (DuPont, USA), Technora (Teijin, Japan), Taparan (Tayho, China), and Heracron (Kolon, Korea) approximate 3.5 GPa [38–40]. The tensile strength of the PA/CNT fiber is superior to that of all these materials, but only when the CNT concentration is high enough. Commercially available pure CNT fibers (DexMat, USA) obtained through wet-spinning process have an electrical conductivity of 10.0 MS m^{-1} [41–43]. The electrical conductivity of the best PA/CNT (10/90) composite fiber is 8.9 MS m^{-1}. However, PA/CNT fibers can compete with pure PA, pure CNT, and other functional fibers when both good mechanical performance and high electrical conductivity are required. Ashby plot in Fig. 5g further indicates that the PA/CNT fibers are better at balancing strength and conductivity than the pure PA and CNT fibers. Other wet-spun pure made of conducting materials like graphene powders [44–46], MXene flakes [47–49], and conjugated polymers [50–52] are currently studied as alternatives to metal-based lightweight products in electrical devices. The physical properties of the PA/CNT fibers described here are considerably superior to those of previously reported synthetic polymer and conducting nanofiller composite fibers [53–55].

The maintenance of the mechanical and electrical properties of PA/CNT (10/90) fibers in extreme conditions can protect people by stably driving the many electronic devices related to life safety systems, such as infrared sensors, communication modules, and gas detectors. For example, an electric circuit can be connected by "DISCO", "VERY", and "DISCOVERY" patterned PA/CNT (10/90) wirings, and tethered with a bulletproof vest (Fig. 6a), fireproof jacket (Fig. 6b) and space suit (Fig. 6c) often used in the harsh conditions. The flame retardant and mechanical robustness of PA/CNT (10/90) fibers can prevent the wiring from snapping due to the fire exposure and violent movement. Figure 6d and S25 show no change in the initial mechanical characteristics of the PA/CNT (10/90) fibers when heated up to 400 °C for 300 min. Above 450 °C, the specific tensile strength starts to decrease after 10 min. The fiber length of 20 mm and the shape of the fiber piece was almost identical before and after exposure to the center of blue zone of the flame, which indicated thermal stability. The PA/CNT (10/90) fibers also possessed a degree of flexure tolerance (Fig. 6e). Fatigue of the metal-based conductors often leads to premature failures early in service life. However, the PA/CNT (10/90) fibers exhibited no change in resistivity under flexure tests, including repeated cycles of twisting, unbending, and folding motions. These results clearly illustrate the potential benefit of PA/CNT (10/90) wiring which requires exceptional flexibility.

Basically, the PA/CNT (10/90) fiber itself was safe to use in our daily lives. When PA/CNT (10/90) fibers were coagulated in an acetone bath, they were subsequently rinsed in a following water bath before winding (Fig. 6f). This process was very important because LLC dope was in an acidic state, and residual CSA on the PA/CNT (10/90) fibers could cause skin corrosion and acute toxicity. However, the CSA was removed when the PA/CNT (10/90) fiber passed through the water bath (stage II). We performed a pH test that indicated the surface of PA/CNT (10/90) fiber was in a neutral state after being cleaned by the water bath (pH = 7). A pH test on the PA/CNT (10/90) fibers immediately after coagulation in the acetone bath (stage I) revealed an acidic state (pH = 2). Furthermore, a lightweight of the PA/CNT (10/90) fibers can accelerate to prospect of replacing metals [56]. As shown in Fig. 6g, the density of PA/CNT (10/90) fiber is 1.84 g cm^{-3}, and this result is lower than the Cu (8.96 g cm^{-3}), aluminum (2.70 g cm^{-3}), and the pure CNT fiber (1.98 g cm^{-3}) [57].

Corrosion is also a significant concern for metallic wires, which react with oxidizing substances in challenging environments. Although the conductors in the electrical cables are protected by insulation, unintended exposures can lead to deterioration in the performance at contact points. Figure 6h showed comparative images of un-insulated Cu wire and PA/CNT fiber exposed to sea water. Deterioration of bare Cu wire was observed within 1 week of immersion, whereas the PA/CNT wire was stable for more than 1 month of testing. Additionally, the mechanical strength and electrical conductivity of PA/CNT wire remained after 30 days of exposure to the various kinds of organic and inorganic solvents (Fig. S26). As shown in Fig. 6i, we fabricated a model of wind turbine. The generated current by converting wind energy into rotating energy of the blade and converting that rotating energy into electrical energy was delivered via the PA/CNT fibers to brighten up the scale model house [58]. The resistance to degradation in corrosive environments of PA/CNT fibers adds to their reliability and promotes to use in renewable energy transportation, including floating solar farms or offshore wind farms which require deployment in media.

Conclusions

The discovery of LLC mesophase driven by the spontaneous molecular self-assembly made PA and CNT possible to proceed the co-processing. The monofilament type of the PA/CNT composite fibers with minimal aggregation were prepared by the continuous wet-spinning, and they provided the broad physical property windows precisely tuned by varying

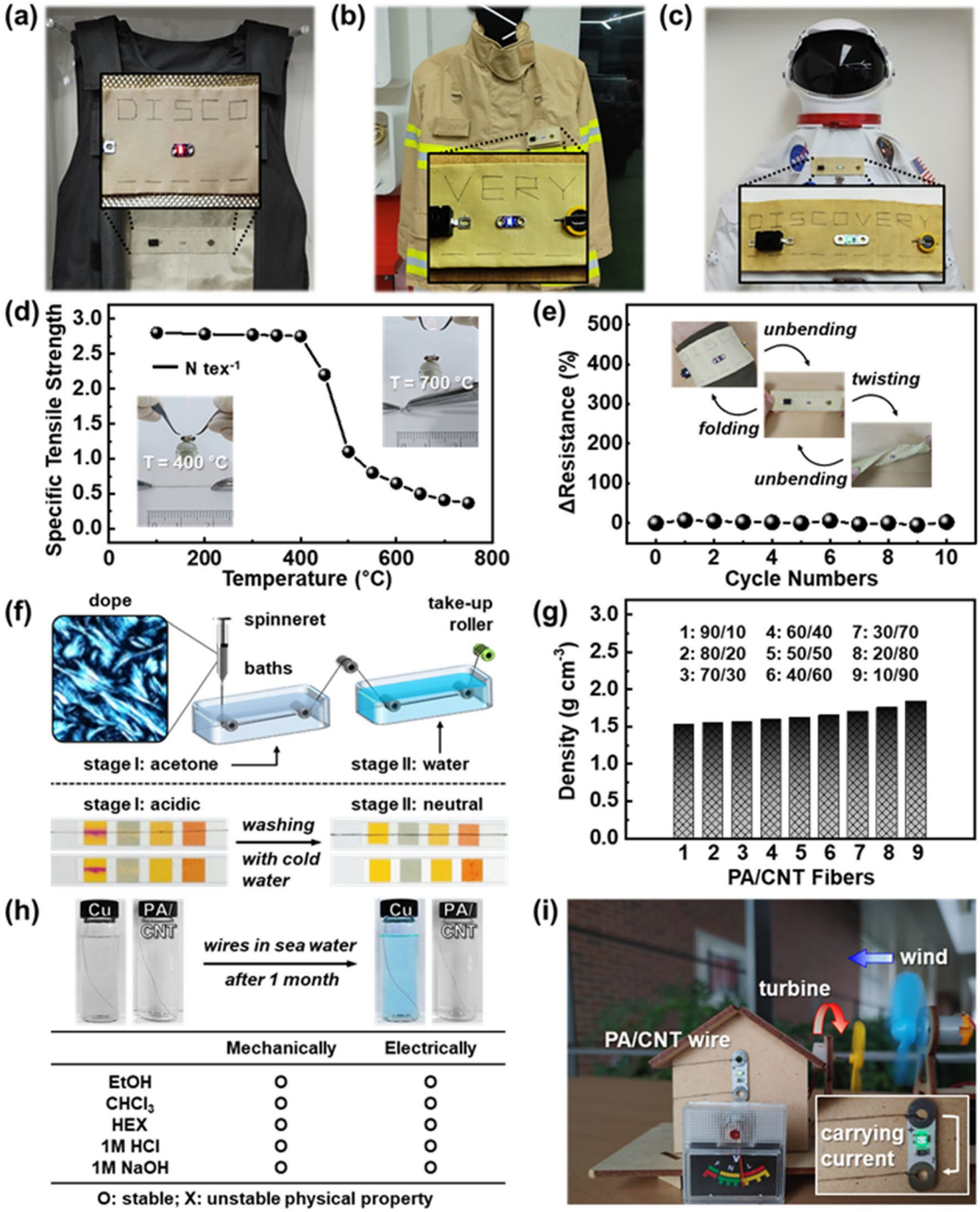

Fig. 6 Macroscopic images of a bulletproof vest (**a**), fireproof jacket (**b**), and spacesuit (**c**) patterned with the PA/CNT fibers for electronic circuits. Thermal stability of the PA/CNT fibers (**d**). Electrical property changes of the PA/CNT fibers stitched into conventional Kevlar fabrics by applying repeated folding, unbending, and twisting motions (**e**). Schematic illustration of the wet-spinning process to obtain a neutral pH state of the PA/CNT fibers for user safety (**f**). Density of the PA/CNT fibers (**g**). Chemical resistance of the PA/CNT fibers (**h**). Model of wind turbine operated by PA/CNT wiring (**i**)

the materials composition, drawing speed, aspect ratio, and phase structures. Furthermore, our results demonstrated that including a small amount of PA in the spinning dope of CNT produced the nanocomposite materials with high tensile strength, electrical conductivity, and electrochemical performance by significantly reducing the internal void

and concomitantly enhancing the orientational order. The lightweight PA/CNT composite fibers with the outstanding chemical, mechanical, and thermal stability can represent an alternative for traditional metal wirings in energy transporting applications.

Supplementary Information The online version contains supplementary material available at https://doi.org/10.1007/s42765-022-00246-4.

Acknowledgements This research was supported by Korea Institute of Science and Technology (KIST) Open Research Program (ORP) and K-Lab Program, and grants from Mid-Career Researcher Program (2021R1A2C2009423), Korea Government MSIT (2021R1R1R1004226), and Korea Research Institute for defense Technology planning and advancement (DAPA KRIT-CT-21-014).

Data availability The data that support the findings of this study are available from the authors upon reasonable request.

Declarations

Conflict of Interest The authors declare no conflict of interests.

References

1. Ye C, Xu Q, Ren J, Liang S. Violin string inspired core-sheath silk/steel yarns for wearable triboelectric nanogenerator applications. *Adv Fiber Mater* **2020**;*2*:24.
2. Kim JG, Yu H, Jung JY, Kim MJ, Jeon DY, Jeong HS, Kim ND. 3D architecturing strategy on the utmost carbon nanotube fiber for ultra-high performance fiber-shaped supercapacitor. *Adv Funct Mater* **2022**;*32*:2113057.
3. Kurzepa L, Lekawa-Raus A, Patmore J, Koziol K. Replacing copper wires with carbon nanotube wires in electrical transformers. *Adv Funct Mater* **2014**;*24*:619.
4. Fang H, Yuan L, Liang G, Gu A. Aramid fibre-based wearable electrochemical capacitors with high energy density and mechanical properties through chemical synergistic combination of multicoatings. *Electrochim Acta* **2018**;*284*:149.
5. Kim DY, Christoff-Tempesta T, Lamour G, Zuo X, Ryu KH, Ortony JH. Morphological transitions of a photoswitchable aramid amphiphile nanostructure. *Nano Lett* **2021**;*21*:2912.
6. Li K, Ni X, Wu Q, Yuan C, Li C, Li D, Chen H, Lv Y, Ju A. Carbon-based fibers: Fabrication, characterization and application. *Adv Fiber Mater* **2022**;*4*:631.
7. Chazot CAC, Damirchi B, Lee B, Duin ACTV, Hart AJ. Molecular alignment of a meta-aramid on carbon nanotubes by in situ interfacial polymerization. *Nano Lett* **2022**;*22*:998.
8. Zhu J, Cao W, Yue M, Hou Y, Han J, Yang M. Strong and stiff aramid nanofiber/carbon nanotube nanocomposites. *ACS Nano* **2015**;*9*:2489.
9. Chen J, Yan L, Song W, Xu D. Interfacial characteristics of carbon nanotube-polymer composites: a review. *Compos Part A* **2018**;*114*:149.
10. Cao W, Yang L, Qi X, Hou Y, Zhu J, Yang M. Carbon nanotube wires sheathed by aramid nanofibers. *Adv Funct Mater* **2017**;*27*:1701061.
11. Xiang S, Zhang N, Fan X. From fiber to fabric: progress towards photovoltaic energy textile. *Adv Fiber Mater* **2021**;*3*:76.
12. Tortora L, Lavrentovich OD. Chiral symmetry breaking by spatial confinement in tactoidal droplets of lyotropic chromonic liquid crystals. *Proc Natl Acad Sci* **2011**;*108*:5163.
13. Vollrath F, Knight DP. Liquid crystalline spinning of spider silk. *Nature* **2001**;*410*:541.
14. Kim DY, Lim SI, Jung D, Hwang JK, Kim N, Jeong KU. Self-assembly and polymer-stabilization of lyotropic liquid crystals in aqueous and non-aqueous solutions. *Liq Cryst Rev* **2017**;*5*:34.
15. Liu H, Tang Y, Wang C, Xu Z, Yang C, Huang T, Zhang F, Wu D, Feng X. A lyotropic liquid-crystal-based assembly avenue toward highly oriented vanadium pentoxide/graphene films for flexible energy storage. *Adv Funct Mater* **2017**;*27*:1606269.
16. Xu Z, Gao C. Graphene chiral liquid crystals and macroscopic assembled fibres. *Nat Commun* **2011**;*2*:571.
17. Zhang J, Uzun S, Seyedin S, Lynch PA, Akuzum B, Wang Z, Qin S, Alhabeb M, Shuck CE, Lei W, Kumbur EC, Yang W, Wang X, Dion G, Razal JM, Gogotsi Y. Additive-free MXene liquid crystals and fibers. *ACS Cent Sci* **2020**;*6*:254.
18. Zeng M, King D, Huang D, Do C, Wang L, Chen M, Lei S, Lin P, Chen Y, Cheng Z. Iridescence in nematics: Photonic liquid crystals of nanoplates in absence of long-range periodicity. *Proc Natl Acad Sci* **2019**;*116*:18322.
19. Choi YJ, Park S, Yoon WJ, Lim SI, Koo J, Kang DG, Park S, Kim N, Jeong KU. Imidazolium-functionalized diacetylene amphiphiles: strike a lighter and wear polaroid glasses to decipher the secret code. *Adv Mater* **2020**;*32*:2003980.
20. Wang P, Barnes B, Wu X, Qu H, Zhang C, Shi Y, Headrick RJ, Pasquali M, Wang Y. Self-sorting of 10-μm-long single-walled carbon nanotubes in aqueous solution. *Adv Mater* **2019**;*31*:1901641.
21. Park SK, Kim SE, Kim DY, Kang SW, Shin S, Kuo SW, Hwang SH, Lee SH, Lee MH, Jeong KU. Polymer-stabilized chromonic liquid-crystalline polarizer. *Adv Funct Mater* **2011**;*21*:2129.
22. Roberts AD, Kelly P, Bain J, Morrison JJ, Wimpenny I, Barrow M, Woodward RT, Gresil M, Blanford C, Hay S, Blaker JJ, Yeates SG, Scrutton NS. Graphene-aramid nanocomposite fibres *via* superacid co-processing. *Chem Commun* **2019**;*55*:11703.
23. Vilatela JJ, Windle AH. Yarn-like carbon nanotube fibers. *Adv Mater* **2010**;*22*:4959.
24. Zhang X, Lu W, Zhou G, Li Q. Understanding the mechanical and conductive properties of carbon nanotube fibers for smart electronics. *Adv Mater* **2020**;*32*:1902028.
25. Zhang S, Zhang F, Pan Y, Jin L, Liu B, Mao Y, Huang J. Multi-wall-carbon-nanotube/cellulose composite fibers with enhanced mechanical and electrical properties by cellulose grafting. *RSC Adv* **2018**;*8*:5678.
26. Jiang X, Gong W, Qu S, Wang D, Liu T, Li Q, Zhou G, Lu W. Understanding the influence of single-walled carbon nanotube dispersion states on the microstructure and mechanical properties of wet-spun fibers. *Carbon* **2020**;*169*:17.
27. Takakura A, Beppu K, Nishihara T, Fukui A, Kozeki T, Namazu T, Miyauchi Y, Itami K. Strength of carbon nanotubes depends on their chemical structures. *Nat Commun* **2019**;*10*:3040.

28. Kim DY, Lee SA, Kim S, Nah C, Lee SH, Jeong KU. Asymmetric fullerene nanosurfactant: Interface engineering for automatic molecular alignments. *Small* **2018**;*14*:1702439.
29. Hong S, Nam J, Park S, Lee D, Park M, Lee DS, Kim ND, Kim DY, Ku BC, Kim YA, Hwang JY. Carbon nanotube fibers with high specific electrical conductivity: synergistic effect of heteroatom doping and densification. *Carbon* **2021**;*184*:207.
30. Sun X, Lu H, Rufford TE, Gaddam RR, Duignan TT, Fan X, Zhao XS. A flexible graphene-carbon fiber composite electrode with high surface area-normalized capacitance. *Sustain Energy Fuels* **1827**;*2019*:3.
31. Kang YS, Jung JY, Choi D, Sohn Y, Lee SH, Lee KS, Kim ND, Kim P, Yoo SJ. Formation mechanism and gram-scale production of PtNi hollow nanoparticles for oxygen electrocatalysis through in situ galvanic displacement reaction. *ACS Appl Mater Interfaces* **2020**;*12*:16286.
32. Cheng Q, Tang J, Ma J, Zhang H, Shinya N, Qin LC. Graphene and carbon nanotube composite electrodes for supercapacitors with ultra-high energy density. *Phys Chem Chem Phys* **2011**;*13*:17615.
33. Sun H, You X, Deng J, Chen X, Yang Z, Ren J, Peng H. Novel graphene/carbon nanotube composite fibers for efficient wire-shaped miniature energy devices. *Adv Mater* **2014**;*26*:2868.
34. Gong S, Zhu ZH. Giant piezoresistivity in aligned carbon nanotube nanocomposite: account for nanotube structural distortion at crossed tunnel junctions. *Nanoscale* **2015**;*7*:1339.
35. Mirri F, Ashkar R, Jamali V, Liberman L, Pinnick RA, Schoot PVD, Talmon Y, Butler PD, Pasquali M. Quantification of carbon nanotube liquid crystal morphology via neutron scattering. *Macromolecules* **2018**;*51*:6892.
36. Behabtu N, Green MJ, Pasquali M. Carbon nanotube-based neat fibers. *Nano Today* **2008**;*3*:24.
37. Bazbouz MB, Aziz A, Copic D, Volder MD, Welland ME. Fabrication of high specific electrical conductivity and high ampacity carbon nanotube/copper composite wires. *Adv Electron Mater* **2021**;*7*:2001213.
38. Şahin K, Clawson JK, Singletary J, Chasiotis I. Shear strength of homopolymer and copolymer aramid fibers. *Polymer* **2020**;*186*:122034.
39. Roenbeck MR, Sandoz-Rosado EJ, Cline J, Wu V, Moy P, Afshari M, Reichert D, Lustig SR, Strawhecker KE. Probing the internal structures of Kevlar fibers and their impacts on mechanical performance. *Polymer* **2017**;*128*:200.
40. Luo L, Yuan Y, Dai Y, Cheng Z, Wang X, Liu X. The novel high performance aramid fibers containing benzimidazole moieties and chloride substitutions. *Mater Des* **2018**;*158*:127.
41. Taylor LW, Williams SM, Yan JS, Dewey OS, Vitale F, Pasquali M. Washable, sewable, all-carbon electrodes and signal wires for electronic clothing. *Nano Lett* **2021**;*21*:7093.
42. Headrick RJ, Tsentalovich DE, Berdequé J, Bengio EA, Liberman L, Kleinerman O, Lucas MS, Talmon Y, Pasquali M. Structure-property relationships in carbon nanotube fibers by downscaling solution processing. *Adv Mater* **2018**;*30*:1704482.
43. Tsentalovich DE, Headrick RJ, Mirri F, Hao J, Behabtu N, Young CC, Pasquali M. Influenced of carbon nanotube characteristics on macroscopic fiber properties. *ACS Appl Mater Interfaces* **2017**;*9*:36189.
44. Yi P, Liu Y, Shi S, Xu Z, Ma W, Wang Z, Liu S, Gao C. Highly crystalline graphene fibers with superior strength and conductivities by plasticization spinning. *Adv Funct Mater* **2020**;*30*:2006584.
45. Xu Z, Liu Y, Zhao X, Peng L, Sun H, Xu Y, Ren X, Jin C, Xu P, Wang M, Gao C. Ultrastiff and strong graphene fibers via full-scale synergetic defect engineering. *Adv Mater* **2016**;*28*:6449.
46. Xin G, Zhu W, Deng Y, Cheng J, Zhang LT, Chung AJ, De S, Lian J. Microfluidics-enabled orientation and microstructure control of macroscopic graphene fiber. *Nat Nanotechnol* **2019**;*14*:168.
47. Shin H, Eom W, Lee KH, Jeong W, Kang DJ, Han TH. Highly electroconductive and mechanically strong $Ti_3C_2T_x$ MXene fibers using a deformable MXene gel. *ACS Nano* **2021**;*15*:3320.
48. Li S, Fan Z, Wu G, Shao Y, Xia Z, Wei C, Shen F, Tong X, Yu J, Chen K, Wang M, Zhao Y, Luo Z, Jian M, Sun J, Kaner RB, Shao Y. Assembly of nanofluidic MXene fibers with enhanced ionic transport and capacitive charge storage by flake orientation. *ACS Nano* **2021**;*15*:7821.
49. Levitt A, Zhang J, Dion G, Gogotsi Y, Razal JM. MXene-based fibers, yarns, and fabrics for wearable energy storage devices. *Adv Funct Mater* **2020**;*30*:2000739.
50. Zhao X, Chen F, Li Y, Lu H, Zhang N, Ma M. Bioinspired ultrastretchable and anti-freezing conductive hydrogel fibers with ordered and reversible polymer chain alignment. *Nat Commun* **2018**;*9*:3579.
51. Zhang J, Seyedin S, Qin S, Lynch PA, Wang Z, Yang W, Wang X, Razal JM. Fast and scalable wet-spinning of highly conductive PEDOT:PSS fibers enables versatile applications. *J Mater Chem A* **2019**;*7*:6401.
52. Uh K, Yoon B, Lee CW, Kim JM. An Electrolyte-free conducting polymer actuator that displays electrothermal bending and flapping wing motions under a magnetic field. *ACS Appl Mater Interfaces* **2016**;*8*:1289.
53. Kim IH, Yun T, Kim JE, Yu H, Sasikala SP, Lee KE, Koo SH, Hwang H, Jung HJ, Park JY, Jeong HS, Kim SO. Mussel-inspired defect engineering of graphene liquid crystalline fibers for synergistic enhancement of mechanical strength and electrical conductivity. *Adv Mater* **2018**;*30*:1803267.
54. Zhou T, Yu Y, He B, Wang Z, Xiong T, Wang Z, Liu Y, Xin J, Qi M, Zhang H, Zhou X, Gao L, Cheng Q, Wei L. Ultra-compact MXene fibers by continuous and controllable synergy of interfacial interactions and thermal drawing-induces stresses. *Nat Commun* **2022**;*13*:4564.
55. Kim JY, Lee W, Kang YH, Cho SY, Jang KS. Wet-spinning and post-treatment of CNT/PEDOT:PSS composites for use in organic fiber-based thermoelectric generators. *Carbon* **2018**;*133*:293.
56. Cesano F, Uddin MJ, Lozano K, Zanetti M, Scarano D. All-carbon conductors for electronic and electrical wiring applications. *Front Mater* **2020**;*7*:219.
57. Subramaniam C, Yamada T, Kobashi K, Sekiguchi A, Futaba DN, Yumura M, Hata K. One hundred fold increase in current carrying capacity in a carbon nanotube-copper composite. *Nat Commun* **2013**;*4*:2202.
58. Lekawa-Raus A, Gizewski T, Patmore J, Kurzepa L, Koziol KK. Electrical transport in carbon nanotube fibres. *Scr Mater* **2017**;*131*:112.